CHEMISTRY

Paralyzed membrane: Current-driven synthesis of a metal-organic framework with sharpened propene/propane separation

Sheng Zhou[1]*, Yanying Wei[1]*, Libo Li[1]*, Yifan Duan[1], Qianqian Hou[1], Lili Zhang[1], Liang-Xin Ding[1], Jian Xue[1], Haihui Wang[1†], Jürgen Caro[2]

Metal-organic framework (MOF) membranes show great promise for propene/propane separation, yet a sharp molecular sieving has not been achieved due to their inherent linker mobility. Here, zeolitic imidazolate framework ZIF-8–type membranes with suppressed linker mobility are prepared by a fast current–driven synthesis (FCDS) strategy within 20 min, showing sharpened molecular sieving for propene/propane separation with a separation factor above 300. During membrane synthesis, the direct current promotes the metal ions and ligands to assemble into inborn-distorted and stiffer frameworks with ZIF-8_Cm (a newly discovered polymorph of ZIF-8) accounting for 60 to 70% of the membrane composition. Molecular dynamics simulations further verify that ZIF-8_Cm is superior to ZIF-8_I $\bar{4}$3m (the common cubic phase) for propene/propane separation. FCDS holds great potential to produce high-quality, ultrathin MOF membranes on a large scale.

INTRODUCTION

High-purity olefins are demanded for the production of bulk chemicals, such as polyethene and polypropene (PP). However, olefin purification from olefin/paraffin mixtures is one of the most energy-intensive processes in the industry, and innovative separations are needed (*1*). Separation of short-chain olefin/paraffin mixtures is currently dominated by cryogenic distillation, which consumes over 120 TBtu (Tera British thermal units) per year (*2*, *3*). Commonly, a two-column–based system with more than 200 trays is required to extract high-purity propene [at least 99.5 weight % for polymer-grade specifications; (*4*)] for PP production. The columns usually range from 70 to 90 m in height and 2 to 6 m in diameter, working with a high reflux ratio of about 15 to 25 and a tray efficiency of 70 to 80%, which makes this process extremely energy expensive (*5*).

An urgent demand for energy-saving propene/propane (C_3H_6/C_3H_8) separation has, thus, spurred researchers to explore various alternatives, and the highly selective permeation based on the molecular sieving membranes seems to be a promising solution (*6*, *7*). Metal-organic frameworks (MOFs) represent a tunable class of porous materials with window aperture size at the molecular scale (*8*, *9*), which are prospective membrane materials (*10*, *11*). One of the star individuals, zeolitic imidazolate framework ZIF-8, whose effective apertures (~4.0 to 4.2 Å) (*12*) fall between the critical diameters of C_3H_6 (~4.0 Å) and C_3H_8 (~4.2 Å) (*13*), is considered as an ideal candidate for C_3H_6/C_3H_8 separation by molecule sieving. However, the commonly prepared thin-layer ZIF-8 membranes do not perform very well, with moderate separation factors below or around 100 (*14*), limiting their application. This situation results mainly from two reasons: (i) the difficulties in controlling polycrystalline membrane microstructures, e.g., the grain boundary, which spoil the selectivity due to the nonselective intercrystalline diffusion (*15*); and (ii) the inherent lattice flexibility (features in soft materials whose linkers are rotatable), which permits larger molecules to permeate through intracrystalline diffusion and decreases the selectivity (*16*).

Often, the grain boundary of a supported thin-layer MOF membrane could be optimized by carefully manipulating and improving the preparation techniques. However, a further enhancement in selectivity is mainly limited by the intrinsic flexible structure of MOFs. Therefore, suppressing linker mobility is an important route to improve ZIF-8's molecular sieving capability (*9*). A very recent study showed a structural transformation of ZIF-8 into polymorphs with more rigid lattices by applying an external electric field (*17*). The newly formed monoclinic Cm and trigonal R3m polymorphs exhibited stiffened networks with hindered linker movements, thus improving molecular sieving of different gas mixtures (*17*). However, about 1 hour after electrical switching off, the rigid ZIF-8_Cm phase disappeared, and the membranes relaxed back into the starting configuration. Recently, He *et al.* (*18*) used an electric field to support the nuclei to deposit onto the support, and then secondary growth was applied to get continuous ZIF-8 membranes, which did not obtain a rigid ZIF-8 polymorph.

Herein, we describe a fast 20-min non-autoclave preparation of ZIF-8 membranes with inborn-suppressed linker mobility by a fast current–driven synthesis (FCDS), where the ZIF-8 membrane is grown by a low direct current (0.7 mA/cm^2). The current-driven synthesized ZIF-8 membrane consists of a mixture of three polymorphs with a majority of the polymorph ZIF-8_Cm and exhibits highly efficient C_3H_6/C_3H_8 separation performance with a separation factor above 300. Molecular dynamics (MD) simulations show that it is the polymorph ZIF-8_Cm with a stiffened lattice that causes the highly selective propene sieving. As shown in Fig. 1A, an electrochemical cell is designed for ZIF-8 membrane growth with a double function of the external direct current. (i) It promotes the deprotonation of the linker 2-methylimidazole (2-MIM) to the imidazolate anion, thus boosting the in situ crystallization of ZIF-8 on the substrate. Simultaneously, Zn^{2+} cations are attracted. This leads to a fast membrane growth at room temperature, and just several minutes are enough for the entire continuous membrane layer to form, showing great scalability potential (Fig. 1, C to H). (ii) The external direct current forms a local in situ electric field (Fig. 1B) and causes inborn lattice distortion of the ZIF-8 lattice, as described in a recent report (*17*), during the assembly of the ZIF-8

[1]School of Chemistry and Chemical Engineering, South China University of Technology, Guangzhou 510640, P. R. China. [2]Institute of Physical Chemistry and Electrochemistry, Leibniz University Hannover, Callinstraße 3A, 30167 Hannover, Germany.
*These authors contributed equally to this work.
†Corresponding author. Email: hhwang@scut.edu.cn

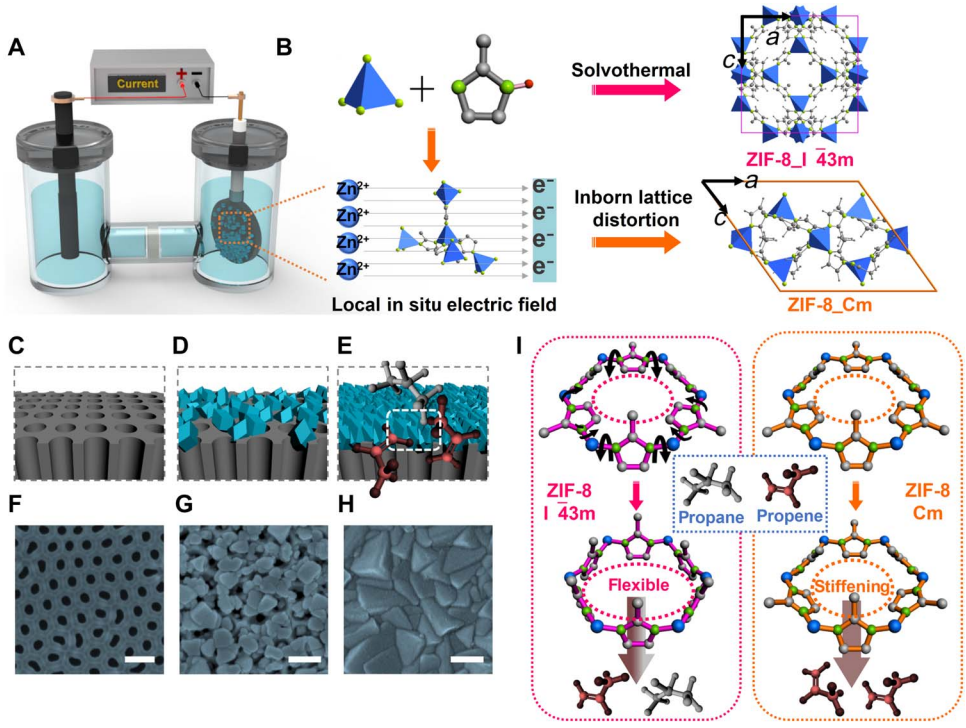

Fig. 1. Synthesis of ZIF-8 membranes and the difference between ZIF-8_I $\bar{4}$3m and ZIF-8_Cm for propene/propane separation. (**A**) The electrochemical cell for membrane growth by FCDS. The substrate serves as a cathode in the electrochemcial system. (**B**) Schematic illustration of the ZIF-8 membrane growth via FCDS in comparison with solvothermal growth. In the solvothermal route, zinc ions and linkers assemble into the normal ZIF-8_I $\bar{4}$3m phase. With the local in situ electric field that formed around the support by the current, inborn lattice distortion occurs and the stiff polymorph ZIF-8_Cm is formed. (**C** to **H**) Schematic illustration and SEM images during ZIF-8 layer formation. Scale bars, 200 nm. (**I**) Difference between ZIF-8_I $\bar{4}$3m and ZIF-8_Cm for C_3H_6/C_3H_8 separation. Because the linkers of ZIF-8_I $\bar{4}$3m are easier to rotate than those of ZIF-8_Cm, during C_3H_6/C_3H_8 separation, the bigger propane molecules can permeate through the ZIF-8_I $\bar{4}$3m apertures more easily than through the ZIF-8_Cm apertures. Consequently, ZIF-8_Cm polymorph is expected to be more efficient for propene sieving.

framework. Therefore, membrane layers of distorted ZIF-8 polymorphs with rigid frameworks and long lifetime can be prepared, which are promising to sharpen molecular sieving capability (Fig. 1I).

RESULTS

The stepwise evolution of ZIF-8 layer formation on the anodic aluminum oxide (AAO; Fig. 1F) is recorded by scanning electron microscopy (SEM) images (Fig. 2 and fig. S1). With a small constant current density of 0.7 mA/cm^2, an initial precursor appears on the surface after ~5 min (fig. S1). The ultrathin precursor is translucent, and the AAO pore structure beneath is visible. However, the precursor does not fully cover the substrate. No crystallinity or specific chemical bonds are detected in this starting period, according to x-ray diffraction (XRD) and Fourier transform infrared (FTIR) spectroscopy (fig. S1, K to M). After an initial nucleation period, the typical crystallization process of MOF formation begins (*19*, *20*). An entire ZIF-8 layer with a thickness of 105 nm is observed after ~8.5 min (Fig. 2A). Once an entire layer is formed, the programmed constant current could not be maintained, and the current signal would drop down at the moment. Because ZIF-8 is nonconductive, the already-formed ZIF-8 membrane serves as an insulating layer to hinder further growth. Therefore, the drop in current is a signal that a complete membrane layer has been formed already (fig. S1). Nevertheless, the current—and thus the growth of the layer—does not stop completely (increasing thickness with time; Fig. 2), despite the growth rate slowing down (fig. S1N). Most probably, in the early stage of layer formation, the precursors could still penetrate through intrinsic defects, such as vacancies and dangling linkers (*21*), to keep contact with the conductive support surface, and self-annealing proceeds. But with longer FCDS time, membrane growth slows and finally stops, even though residual nutrients remain in the mother solution (both ligands and metal ions can be detected; fig. S2). The ZIF-8 layer grown for 20 min displays a thickness of approximately 200 nm (Fig. 2, D and H), which is much thinner than most other reported ZIF-8 membranes. Moreover, an elegant thin-film interference phenomenon is also observed (fig. S3A), agreeing well with the thickness shown in Fig. 2D (*22*). The deposited ZIF-8 film attaches well to the supports, and it did not flake off even under an ultrasonic water bath treatment for 60 min. As shown in fig. S3 and movie S1, the thin-film interference still exists after ultrasonic treatment, and no visible cracking appears. The appearance of the membranes remained unchanged after strenuous shaking and even falling from a height of 1 m. This high durability of the membranes allowed us to handle and measure them easily.

The growth mechanism of FCDS is investigated by electrochemical methods. In principle, the deprotonation of the ligands is a vital step for the assembly of MOF crystals. Dincă and co-workers (*23*) proposed that during cathodic deposition, the existence of NO_3^- or other probases in the solution is necessary to generate a base for the in situ deprotonation of the ligands. However, all previous cathodic deposition reports focused on carboxylate-based MOFs, and no azolate-based MOFs (such as ZIF-8) have been grown at the cathode before (*24*). In our case, the matter is different, because $Zn(CH_3COO)_2$ instead of

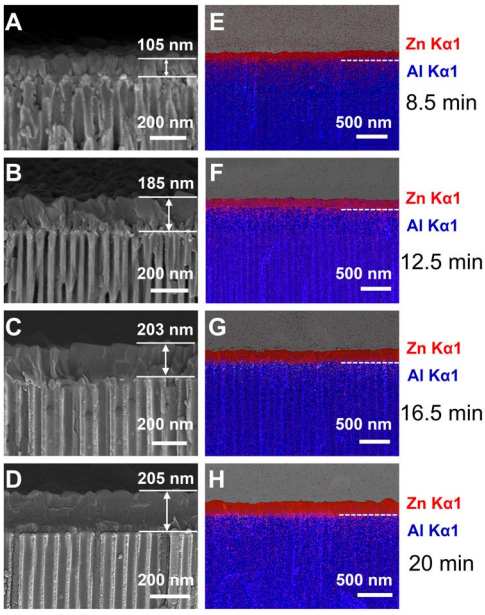

Fig. 2. SEM characterization of FCDS membranes. (**A** to **D**) Cross-sectional SEM images of FCDS ZIF-8 membranes with different growth times. (**E** to **H**) Energy-dispersive x-ray spectroscopy (EDXS) mapping images of the membranes' cross-sectional view at lower magnification (due to the difficulty to scan at higher magnification). Zn (red) is the tracer for the ZIF-8 layer, and Al (blue) is the tracer for the AAO support. The corresponding membrane SEM images with lower magnification are given in fig. S1.

$Zn(NO_3)_2$ was used. To reveal the intrinsic mechanism, the mother solution of 0.05 M zinc acetate and 0.1 M 2-MIM in methanol was characterized by cyclic voltammetry (CV; fig. S4). Only the H_2 evolution reaction was found to occur (fig. S4B), indicating that the ZIF-8 formation is directly related to the reduction of protons. We speculate that protons in 2-MIM are removed and reduced by electrons (eq. i), although a slight H_2 evolution reaction is also observed in pure methanol (eq. ii; fig. S4C). Because the p*K*a (acidity coefficient; where *K*a is the acid dissociation constant) value of 2-MIM (14.44 ± 0.10) (*25*) is lower than that of methanol (15.17 ± 0.10) (*25*), the H^+ dissociation from the 2-MIM ligands is much easier, and the 2-MIM/methanol solution shows higher electrical conductivity (fig. S4E) and larger current density by linear sweep voltammetry (LSV; fig. S4, C and D). These results confirm that the ligands provide protons. Consequently, the deprotonated ligands can easily coordinate with the Zn^{2+} ions to form ZIF-8.

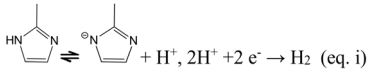

$$CH_3OH \rightleftharpoons CH_3O^{\ominus} + H^+,\ 2H^+ + 2e^- \rightarrow H_2 \quad \text{(eq. ii)}$$

Gas separation through a series of five ZIF-8 membranes with different FCDS times was measured by the Wicke-Kallenbach technique (fig. S5). Longer FCDS time results in higher C_3H_6/C_3H_8 separation factors (Fig. 3A), and the membranes grown for 20 min exhibit separation factors of 304.8 with C_3H_6 permeance of 52.0 gas permeation units (GPUs; 1 GPU = 3.348×10^{-10} mol m^{-2} s^{-1} Pa^{-1}, average values of nine independent preparations from 12 samples; table S1). The selectivity does not continue to increase even if the growth time exceeds 20 min. The membrane selectivity is significantly higher (the best up to date) than other membranes (Fig. 3B). Considering the linker movements, it is hard for phase-pure ZIF-8 membranes that are prepared by usual solvothermal crystallization to have such an unprecedented separation factor (*12*). Thus, the improved selectivity can be ascribed to the suppressed linker mobility in the current-driven synthesized membranes, since a local in situ electric field exists during FCDS of ZIF-8. Therefore, we expected that a stiffer ZIF-8 polymorph might have been formed, analogous to the previous report on switching of a ZIF-8 layer by an external electric field (*17*). Rietveld refinement of the XRD results using TOPAS 4.1 shows that the ZIF-8 membranes are a mix of three phases with different space groups: Cm, R3m, and I$\bar{4}$3m (Fig. 4A and fig. S6). These three polymorphs of ZIF-8 are also observed when ZIF-8 is exposed to an external electric field (*17*). For the membrane grown for 20 min, more than 70% of the ZIF-8 crystals belong to the stiffer Cm phase, while the flexible I$\bar{4}$3m phase only accounts for less than 5% (Fig. 4A). The superior selectivity, $S_{propene/propane}$, of ZIF-8_Cm to ZIF-8_I $\bar{4}$3m is confirmed by MD simulations based on both a single monolayer and a 200-nm-thick membrane of ZIF-8 (fig. S7, Fig. 4B, and tables S4 and S5). The root mean square deviation (RMSD) of the ZIF-8_Cm membrane in the MD simulations is about half of that of the ZIF-8_I $\bar{4}$3m membrane (fig. S7A), which indicates that the linker movements in ZIF-8_Cm are suppressed, agreeing with the recent report (*17*). Because of the suppressed linker movement of ZIF-8_Cm, the passage rate of propene through the membrane decreases to about 31% of that through ZIF-8_I$\bar{4}$3m, while a more drastic decrease to 8.7% of the original value is observed for propane. The decrease of passage rate is consistent with the moderate permeances of the membranes. However, this asynchronism of rate changes leads to a considerably enhanced C_3H_6/C_3H_8 selectivity of ZIF-8_Cm (~530), which is much higher than that of ZIF-8_I$\bar{4}$3m (~150). The ZIF-8 membranes synthesized in our work consist of ~70% ZIF-8_Cm; thus, the ideal selectivity could be roughly estimated to be ~370 (530 × 70%) according to the MD simulation results, which is slightly higher than the experimental value of 305.

The benefits of suppressed linker mobility in ZIF-8_Cm–dominated membranes are reflected by the separation performance of membranes grown for different times (Fig. 3A), such as 8.5, 12.5, 16.5, 25, and 30 min. In all these current-driven synthesized membranes, the ZIF-8_Cm phase dominates with a share of 60 to 70% (fig. S6). For extended FCDS time (from 8.5 to 30 min), the separation factor increases steadily from 128 to above 300, while the permeance slightly decreases. All separation factors are superior to literature data, which proves that ZIF-8_Cm–dominated membranes are better candidates for propene purification. For a better comparison, we also prepared ZIF-8 membranes by traditional solvothermal growth, which were dominated by the ZIF-8_I $\bar{4}$3m phase (fig. S6G). However, the propene/propane separation factor is only around 7 (fig. S5G), similar to the recent report (*17*).

Moreover, the increase of the separation factor with increasing FCDS time is attributed to the current-driven mending of intrinsic defects and grain boundary structure. The evidence can be found from laser scanning confocal microscopy (LSCM) images of membranes prepared for different FCDS times (*15*). Extending the preparation time from 5 to 7 min, fewer and fewer probe molecules (CdTe quantum dots) could be detected in the permeate surface of membranes, showing abatement of intercrystalline defects with time. After 8.5 min of FCDS, no intercrystalline defects could be detected (fig. S8), which demonstrates that the membrane quality is self-reinforced during membrane evolution. Simultaneously, extended growth results in a higher framework density at the grain boundary region with larger mass transfer resistance,

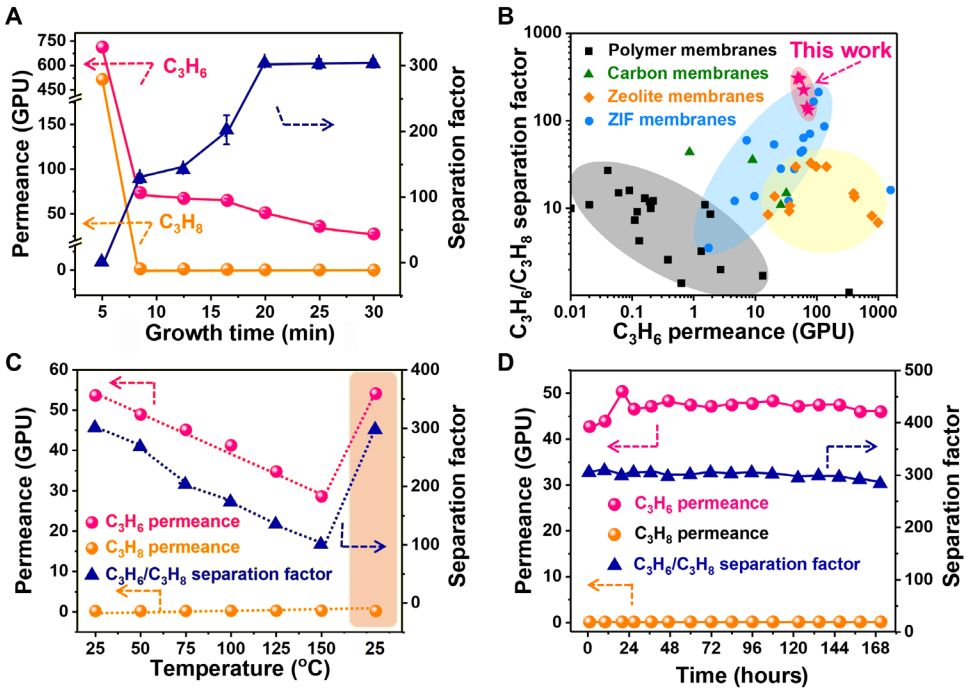

Fig. 3. Membrane separation performance. (**A**) Binary C_3H_6/C_3H_8 separation performance of the ZIF-8 membranes as a function of growth time at room temperature. (**B**) Comparison of the C_3H_6/C_3H_8 separation performance of FCDS ZIF-8 membranes with literature data. Information on the data points is given in table S3. (**C**) Binary C_3H_6/C_3H_8 separation performances of the ZIF-8 membrane (grown for 20 min) as a function of temperature. The rectangular orange area shows the separation performance after cooling to 25° from 150°C. (**D**) Long-term stability of the ZIF-8 membrane (grown for 20 min) for C_3H_6/C_3H_8 separation at room temperature and 1 bar.

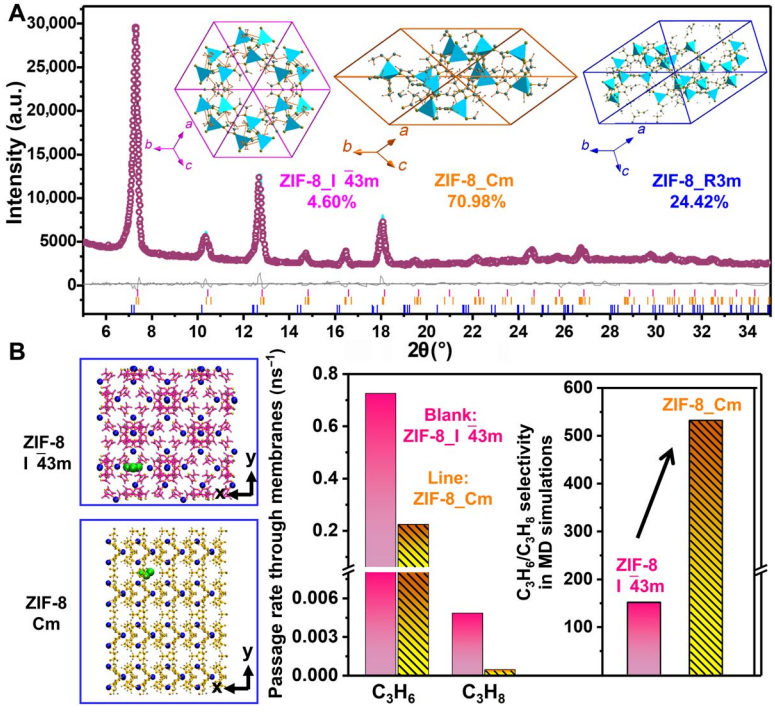

Fig. 4. XRD Rietveld refinement and MD simulations results. (**A**) Rietveld refinement of the XRD results of FCDS ZIF-8 membranes grown for 20 min. [Rwp (weighted profile R factor), 3.30%; Rexp (expected profile R factor), 1.74%; GoF (goodness of fit), 1.90]. The results show that the main phase in the as-synthesized membranes is ZIF-8_Cm, so the membrane separation performance is mainly determined by ZIF-8_Cm. a.u., arbitrary unit. (**B**) MD simulations of a propene/propane molecule passing through a ZIF-8_I$\bar{4}$3m or ZIF-8_Cm membrane with a thickness (along the *z* axis) of 200 nm, respectively. The passage rate (the inverse of passage time, averaged from five independent MD simulations in table S5) of both propene and propane through the ZIF-8_Cm membrane is slower than that through the ZIF-8_I$\bar{4}$3m membrane. This decrement is less significant for propene, leading to a considerably enhanced selectivity of propene over propane (increased from ~150 to ~530).

as previously reported in both zeolite (*26*) and MOF membranes (*27*, *28*). Thus, the permeances of both C_3H_6 and C_3H_8 decrease with time, even though the thickness does not considerably increase. Moreover, the permeance of C_3H_6 decreases slightly with increasing feed pressure (1.0 to1.4 atm; fig. S5E), which is in accordance with the literature (*15*). The selectivity shows negligible changes, indicating lack of defects and suppressed flexibility. The C_3H_6 permeance decreases with increasing temperature (measured from 25° to 150°C), while the C_3H_8 permeance slightly increases, leading to a decreased separation factor (Fig. 3C). This trend is analogous to common ZIF-8 membranes for C_3H_6/C_3H_8 separation, as the gas permeation through membranes is an activated process composed of molecular adsorption and diffusion (*29*). Considering the difference of the apparent activation energy of the gas permeation between C_3H_6 and C_3H_8 (fig. S5F), this trend is quite reasonable. Rietveld refinement of XRD results shows that the ZIF-8_Cm phase still accounts for ~70% of membrane composition after heating at 150°C for 24 hours, and the separation performance can totally turn back after cooling to room temperature (fig. S6F and Fig. 3C). This means that a higher temperature does not cause relaxation, and the ZIF-8_Cm polymorph is temperature stable, at least up to 150°C. In addition, the ZIF-8 membrane also exhibits good stability over a 170-hour long-term C_3H_6/C_3H_8 separation experiment (Fig. 3D), indicating the high quality of the membrane and long lifetime of ZIF-8_Cm. It should be noted that, different from the previous work (*17*), the ZIF-8_Cm polymorph obtained by inborn distortion in this work will not turn to ZIF-8_I$\bar{4}$3m, because it is the parent form and any further change of the original configuration needs extra energy.

Besides (i) perfect defect-free growth and (ii) growing the polymorph with rigid lattice and molecular sieve property, FCDS holds great promise for a scale up. In contrast to the conventional solvothermal growth, which requires autoclaves because of relatively high temperature, high pressure, and long reaction time, the straightforward one-step and mild FCDS strategy exhibits an ultrafast route for membrane preparation at ambient conditions (fig. S9), which is beneficial for reducing the cost and energy consumption with improved productivity and safety. Moreover, the generality of the FCDS for ZIF-8 membranes on different conducting substrates has also been verified, proven for stainless steel nets, nickel foam, and porous stainless steel discs with ZIF-8_Cm polymporph still dominating the membrane composition (fig. S10), which makes the FCDS strategy more industrially applicable and flexible.

In summary, a ZIF-8 layer with inborn-suppressed linker mobility has been synthesized successfully by an electrochemical method named "fast current driven synthesis" (FCDS), leading to sharpened molecular sieving capability for C_3H_6/C_3H_8 separation. The XRD Rietveld refinement results reveal that approximately 60 to 70% of the current-driven synthesized ZIF-8 belongs to the ZIF-8_Cm polymorph, whose framework structure is stiffer than that of the common ZIF-8_I$\bar{4}$3m phase. The benefits of the supressed linker mobility in ZIF-8_Cm for C_3H_6/C_3H_8 separation are proven by both mixed-gas permeation experiments and MD simulations, where ZIF-8_Cm–dominated membranes exhibit a highly enhanced C_3H_6/C_3H_8 separation factor above 300. Moreover, stepwise evolution of membranes with FCDS time demonstrates the self-reinforced process during membrane growth using the FCDS route. This strategy is not only facile, mild, and straightforward but also a general tool for the large-scale production of high-quality MOF membranes for gas separation.

DISCUSSION

Here, we prepared FCDS membranes on planar conducting supports such as metal-coated AAO, stainless steel nets, Ni foam, and porous stainless steel discs. For industrial applications, the permeance, in particular, must be improved. Increasing the effective membrane area per volume will be one route to increase the yield of the target product, and fabricating hollow fiber membranes may be an effective approach. FCDS can be applied to conductive hollow fiber supports, as shown in fig. S10J. The ZIF-8 layer could be controlled to grow either on the inner surface or on the outer surface by simply tuning the location of the conductive surface. Of course, it will be a challenging task to develop a cheap conductive hollow fiber from conducting polymers or ceramics. Conductive TiO_2 or mixed matrices of ceramic powder and metal powder could also be used.

MATERIALS AND METHODS

Materials

Zinc acetate dehydrate (>99.99%, Aladdin), 2-MIM (>99%, Aladdin), methanol (Guangzhou Donghong Chemical Reagent Co. Ltd.), tetrabutylammonium hexafluorophosphate [$(NBu_4)PF_6$; >99.99%, Aladdin], zincon monosodium salt (Sino Chemical Co. Ltd.), and porous AAO (diameter, 18 mm; pore diameter, 70 nm; Pu-Yuan Nanotechnology Limited Company) were used in this study. Asymmetric ceramic support discs (α-Al_2O_3 support with 70-nm grains in the top layer) with a diameter of 18 mm were purchased from IKTS (Fraunhofer Institute for Ceramic Technologies and Systems) Hermsdorf. An HDV-7C potentiostat from Fujian Changlian Electronic Co. Ltd was used.

Methods

Preparation of the 2-MIM solution

First, 0.41 g of 2-MIM was dissolved in 50 ml of methanol and then treated by ultrasonication to dissolve all the chemicals. The electrical conductivity of this solution was measured by a conductivity meter at room temperature.

Preparation of the $(NBu_4)PF_6$ solution with the same electrical conductivity as the 2-MIM solution

First, 50 ml of methanol was poured into a flask containing the probe of the conductivity meter. Then, $(NBu_4)PF_6$ powder was added into the solution with gentle shaking until the electrical conductivity reached that of the 2-MIM solution.

Preparation of mother solution for synthesis of ZIF-8 membranes

A solid mixture of zinc salts (0.55 g of zinc acetate) and 0.41 g of 2-MIM was dissolved in 50 ml of methanol. The molar ratio of 2-MIM/ Zn^{2+} in this system was 2:1. The mixed solution was treated by ultrasonication to dissolve all the chemicals.

Preparation of ultrathin ZIF-8 membranes by FCDS

An AAO disc with a Pt coating was immerged into the mother solution prepared as stated above. A current density of –0.7 mA cm^{-2} was conducted for a certain period at room temperature to generate the ultrathin ZIF-8 membranes before the membranes were taken out and dried at room temperature.

Preparation of ultrathin ZIF-8 layers by FCDS on stainless steel nets, Ni foam, and porous stainless steel discs

The substrates (stainless steel nets, Ni foam, or porous stainless steel discs) were first cleaned with diluted HCl solution and ethanol and then were immersed the mother solution prepared as stated above. A current

was applied for 20 min at room temperature with a density of −0.7 mA cm^{-2} to generate ultrathin ZIF-8 layers before they were taken out and dried at room temperature.

Preparation of ZIF-8 membranes by solvothermal growth

The growth method reported in (*17*) was adopted. First, the support of Al_2O_3 was soaked for 1 hour in a solution containing 0.982 g of $ZnCl_2$, 2.142 g of $Zn(NO_3)_2{\cdot}6H_2O$, and 26.6 ml of MeOH. Afterward, the support was transferred into a PTFE (polytetrafluoroethylene) holder and set vertically in a PTFE-lined autoclave containing 0.509 g of sodium formate, 5.19 g of 2-MIM, and 40 ml of MeOH. The reaction mixture was heated to 120°C and held at that temperature for 8 hours.

Characterization

XRD patterns were recorded at room temperature under ambient conditions with a Bruker D8 Advance diffractometer with Cu Ka radiation at 40 kV and 40 mA. To get enough intensity for Rietveld refinement, the samples were scanned at 75 s per step, where normal scanning was at 15 s per step. Calculations on the XRD patterns were performed with TOPAS 4.1 using equipment-specific correction parameters. An *xyz* profile function was used to fit the peak shapes. FTIR patterns were recorded with a Bruker VERTEX 70 spectrometer. Ultraviolet-visible spectroscopy was characterized using a SHIMADZU UV-2450. The morphologies and cross sections of the membranes were observed by SEM using a HITACHI SU8200. The electrical conductivity was measured at room temperature with a conductivity meter produced by INESA Scientific Instrument Co. Ltd. (DDS-307A). CV and LSV were characterized using an electrochemical workstation produced by CH Instruments Inc. (CHI 760E). The LSCM images were characterized by Leica TCS SP8.

LSCM measurements on ZIF-8 membranes for different growth times were conducted to detect the intercrystalline defects according to the literature (*15*, *30*). The membranes were mounted on homemade permeance cells. The membrane side was contacted to pure methanol, while the support side was saturated with the methanol solution containing CdTe quantum dots (~2.8 nm; supplied by Nanjing beri Instrument Equipment Co. Ltd.) for a period of 60 hours. Then, the solutions in both sides were poured out, and the membranes were removed, washed with copious amount of fresh methanol, dried by blowing N_2 gas, and kept at room temperature for 12 hours before the characterization.

Gas permeation test

For a single-gas permeation measurement, the prepared MOF membrane was fixed in a module sealed with O-rings. A volumetric flow rate of 25 ml min^{-1} gas was applied to the feed side of the membrane, and the permeate gas was removed from the permeate side by the sweep gas. Pressures at both the feed side and the permeate side were maintained at 1 bar. In most cases, N_2 was used as the sweep gas, except in the N_2 single-gas measurement, where CH_4 was used as the sweep gas. A calibrated gas chromatograph (Agilent 7890A) was used to measure the concentration of each gas on the permeate side. The membrane permeance, P_i (mol m^{-2} s^{-1} pa^{-1}), is defined as Eq. 1

$$P_i = \frac{N_i}{\Delta P_i \bullet A} \tag{1}$$

where N_i (mol s^{-1}) is the molar flow rate of component *i*, ΔP_i (Pa) is the transmembrane pressure difference of component *i*, and *A* (m^2) is the effective membrane area for testing. The ideal selectivity, $S_{i/j}$, is calculated from the relation between the permeance of components *i* and *j*.

$$S_{i/j} = \frac{P_i}{P_j} \tag{2}$$

For the mixed-gas permeation measurement, the prepared MOF membrane was fixed in a module sealed with O-rings. A 1:1 mixture of gas was applied to the feed side of the membrane, and the permeate gas was removed from the permeate side by the sweep gas. The feed flow rate was kept constant with a total volumetric flow rate of 50 ml min^{-1} (each gas, 25 ml min^{-1}). Pressures at both the feed side and the permeate side were maintained at 1 bar. N_2 was used as the sweep gas. A calibrated gas chromatograph was used to measure the concentration of each gas on the permeate side. The separation factor, $\alpha_{i,j}$, of the gas pairs is defined as the quotient of the molar ratios of the components (*i*, *j*) in the permeate side, divided by the quotient of the molar ratios of the components (*i*, *j*) in the feed side

$$\alpha_{i/j} = \frac{X_{i,\mathrm{perm}}/X_{j,\mathrm{perm}}}{X_{i,\mathrm{feed}}/X_{j,\mathrm{feed}}} \tag{3}$$

MD simulation method

First, the simulation system consisted of a single monolayer ZIF-8 nanosheet and a gas molecule. ZIF-8 was modeled by force field parameters developed by Economou and co-workers (*13*, *31*), while gas molecules were modeled by the united atom Trappe force field (*32*, *33*). The crystal structures of ZIF-8 were taken from the recent publication (*17*). The periodic boundary condition (PBC) was applied to the *xy* direction of the system (the membrane plane), and the wall condition was applied to the *z* direction (vertical to the membrane plane). In the beginning, a gas molecule was put near the ZIF-8 nanosheet. The system was subjected to a 500-step steepest-descent energy minimization, and then an NVT (constant particle number, volume, and temperature) simulation was performed (leapfrog algorithm with a time step of 1 fs). The ZIF-8 nanosheet was flexible during the NVT simulation. The Nose-Hoover thermostat (*34*) was used to maintain a constant simulation temperature of 298.2 K. The short-range interactions were evaluated using a neighbor list of 10 Å that was updated every 10 steps, and the Lennard-Jones interactions were switched off smoothly between 8 and 9 Å. A long-range analytical dispersion correction was applied to the energy to account for the truncation of these interactions (*35*). The electrostatic interactions were evaluated using the reaction field method (*36*). In a normal NVT simulation where no pulling force was applied to the gas molecule, it could not pass the membrane even though the simulation time was extended to 500 ns. This is quite expected, since the size of gas molecules (propane, ~0.42 nm; propene, ~0.40 nm) was considerably larger than the window size of ZIF-8 (0.34 nm, with the flexibility of ZIF-8 taken into account). Thus, we applied a constant force of 50 kJ/(mol nm) to the gas molecule during the following NVT simulations, where the gas molecule passed through the membrane during a time course ranging from 0.1 to 50 ns, which depends on the specific gas molecule and the ZIF-8 phase. As for each specific gas molecule (propane or propene) + ZIF-8 phase ($I\bar{4}3m$ or Cm) membrane system, the simulation was repeated five times, and the average time it took the gas molecule to pass through the membrane was reported (table S4). The permeability was defined

as the reciprocal of the time course, and the selectivity was defined as the ratio of permeability between propane and propene.

$$S_{\text{propene/propane}} = \frac{P_{\text{propene}}}{P_{\text{propane}}}$$

To better mimic the experiments, the other set of simulations were also performed, where a propane/propene molecule moved in bulk ZIF-8 membrane ($I\bar{4}3m$ or Cm phase) (PBC was applied to all *xyz* directions). A constant force of 100 kJ/(mol nm) was exerted to the gas molecule, and the time course it took to move 200 nm along the membrane thickness direction (z) was recorded (table S5).

The bulk modulus of the single monolayer and 200-nm-thick membrane was calculated from the fluctuation of the membrane volume

$$K_{\text{bulk}} = k_B T V / \sigma_V^2$$

where K_{bulk} is the bulk modulus, V is the volume of the membrane, k_B is Boltzmann's constant, T is the temperature, and σ_V^2 is the variance of the volume.

SUPPLEMENTARY MATERIALS

Supplementary material for this article is available at http://advances.sciencemag.org/cgi/content/full/4/10/eaau1393/DC1

Fig. S1. SEM images and XRD and FTIR results and change of membrane thickness with time.
Fig. S2. Detection of the remaining metal ions and ligands in the spent growth solution.
Fig. S3. Illustration of thin film interference and the excellent durability of ZIF-8 membranes.
Fig. S4. Electrochemical characterization of growth mechanism.
Fig. S5. Gas permeation setup and properties.
Fig. S6. Rietveld refinement results of different ZIF-8 membranes.
Fig. S7. MD simulation results.
Fig. S8. LSCM characterization of self-elimination of defects.
Fig. S9. Comparison of the time needed for the fabrication of MOF membranes.
Fig. S10. SEM images and phase composition of the ZIF-8 layers grown on different conductive substrates and potential concept of hollow fiber formats.
Table S1. C_3H_6/C_3H_8 separation properties for the ZIF-8 membranes prepared by FCDS grown at different times in a solution containing $Zn(CH_3COO)_2$ at room temperature and 1 bar with a 1:1 binary mixture of C_3H_6 and C_3H_8.
Table S2. Detailed comparison of the synthesis time, methods, fabrication conditions, and their C_3H_6/C_3H_8 separation factors for different ZIF-8 membranes.
Table S3. Detailed C_3H_6/C_3H_8 separation performance of different membranes listed in Fig. 3B.
Table S4. Detailed results of MD simulations of gas passing through a single monolayer of ZIF-8 (each ZIF-8_$I\bar{4}3m$/Cm + propene/propane system was simulated for five times, and the averaged result was reported).
Table S5. Detailed results of MD simulations of gas passing through 200-nm-thick membranes of ZIF-8 (each ZIF-8_$I\bar{4}3m$/Cm + propene/propane system was simulated for five times, and the averaged result was reported).
Movie S1. Durability test by ultrasonic water bath treatment, shaking, and falling test.
References (*37*–*59*)

REFERENCES AND NOTES

1. D. S. Sholl, R. P. Lively, Seven chemical separations: To change the world: Purifying mixtures without using heat would lower global energy use, emissions and pollution—And open up new routes to resources. *Nature* **532**, 435–438 (2016).
2. S. Robinson, R. Jubin, B. Choate, Materials for Separation Technology: Energy and Emmision Reduction Opportunities. *Washington DC: US Dept. of Energy*, (2005).
3. J. E. Bachman, Z. P. Smith, T. Li, T. Xu, J. R. Long, Enhanced ethylene separation and plasticization resistance in polymer membranes incorporating metal-organic framework nanocrystals. *Nat. Mater.* **15**, 845–849 (2016).
4. A. Cadiau, K. Adil, P. Bhatt, Y. Belmabkhout, M. Eddaoudi, A metal-organic framework–based splitter for separating propylene from propane. *Science* **353**, 137–140 (2016).
5. F. A. Da Silva, A. E. Rodrigues, Propylene/propane separation by vacuum swing adsorption using 13X zeolite. *AIChE J.* **47**, 341–357 (2001).
6. K. Varoon, X. Zhang, B. Elyassi, D. D. Brewer, M. Gettel, S. Kumar, J. A. Lee, S. Maheshwari, A. Mittal, C.-Y. Sung, M. Cococcioni, L. F. Francis, A. V. McCormick, K. A. Mkhoyan, M. Tsapatsis, Dispersible exfoliated zeolite nanosheets and their application as a selective membrane. *Science* **334**, 72–75 (2011).
7. M. Y. Jeon, D. Kim, P. Kumar, P. S. Lee, N. Rangnekar, P. Bai, M. Shete, B. Elyassi, H. S. Lee, K. Narasimharao, S. N. Basahel, S. Al-Thabaiti, W. Xu, H. J. Cho, E. O. Fetisov, R. Thyagarajan, R. F. Dejaco, W. Fan, K. A. Mkhoyan, J. I. Siepmann, M. Tsapatsis, Ultra-selective high-flux membranes from directly synthesized zeolite nanosheets. *Nature* **543**, 690–694 (2017).
8. H. Furukawa, K. E. Cordova, M. O'Keeffe, O. M. Yaghi, The chemistry and applications of metal-organic frameworks. *Science* **341**, 1230444 (2013).
9. C. Zhang, W. J. Koros, Zeolitic imidazolate framework-*enabled* membranes: Challenges and opportunities. *J. Phys. Chem. Lett.* **6**, 3841–3849 (2015).
10. J. Gascon, F. Kapteijn, Metal-organic framework membranes—High potential, bright future? *Angew. Chem. Int. Ed.* **49**, 1530–1532 (2010).
11. T. Rodenas, I. Luz, G. Prieto, B. Seoane, H. Miro, A. Corma, F. Kapteijn, F. X. Llabrés I Xamena, J. Gascon, Metal–organic framework nanosheets in polymer composite materials for gas separation. *Nat. Mater.* **14**, 48–55 (2015).
12. C. Zhang, R. P. Lively, K. Zhang, J. R. Johnson, O. Karvan, W. J. Koros, Unexpected molecular sieving properties of zeolitic imidazolate framework-8. *J. Phys. Chem. Lett.* **3**, 2130–2134 (2012).
13. P. Krokidas, M. Castier, S. Moncho, E. Brothers, I. G. Economou, Molecular simulation studies of the diffusion of methane, ethane, propane, and propylene in ZIF-8. *J. Phys. Chem. C* **119**, 27028–27037 (2015).
14. M. J. Lee, H. T. Kwon, H.-K. Jeong, High-flux zeolitic imidazolate framework membranes for propylene/propane separation by postsynthetic linker exchange. *Angew. Chem. Int. Ed.* **57**, 156–161 (2018).
15. L. Sheng, C. Wang, F. Yang, L. Xiang, X. Huang, J. Yu, L. Zhang, Y. Pan, Y. Li, Enhanced C_3H_6/C_3H_8 separation performance on MOF membranes through blocking defects and hindering framework flexibility by silicone rubber coating. *Chem. Commun.* **53**, 7760–7763 (2017).
16. L. Diestel, H. Bux, D. Wachsmuth, J. Caro, Pervaporation studies of *n*-hexane, benzene, mesitylene and their mixtures on zeolitic imidazolate framework-8 membranes. *Microporous Mesoporous Mater.* **164**, 288–293 (2012).
17. A. Knebel, B. Geppert, K. Volgmann, D. Kolokolov, A. Stepanov, J. Twiefel, P. Heitjans, D. Volkmer, J. Caro, Defibrillation of soft porous metal-organic frameworks with electric fields. *Science* **358**, 347–351 (2017).
18. G. He, M. Dakhchoune, J. Zhao, S. Huang, K. V. Agrawal, Electrophoretic nuclei assembly for crystallization of high-performance membranes on unmodified supports. *Adv. Funct. Mater.* **28**, 1707427 (2018).
19. B. Seoane, J. M. Zamaro, C. Tellez, J. Coronas, Sonocrystallization of zeolitic imidazolate frameworks (ZIF-7, ZIF-8, ZIF-11 and ZIF-20). *CrstEngComm* **14**, 3103–3107 (2012).
20. E. Haque, N. A. Khan, J. H. Park, S. H. Jhung, Synthesis of a metal–organic framework material, iron terephthalate, by ultrasound, microwave, and conventional electric heating: A kinetic study. *Chemistry* **16**, 1046–1052 (2010).
21. C. Zhang, C. Han, D. S. Sholl, J. R. Schmidt, Computational characterization of defects in metal–organic frameworks: Spontaneous and water-induced point defects in ZIF-8. *J. Phys. Chem. Lett.* **7**, 459–464 (2016).
22. E. Barankova, X. Tan, L. F. Villalobos, E. Litwiller, K.-V. Peinemann, A metal chelating porous polymeric support: The missing link for a defect-free metal–organic framework composite membrane. *Angew. Chem. Int. Ed.* **56**, 2965–2968 (2017).
23. M. Li, M. Dincă, Reductive electrosynthesis of crystalline metal–organic frameworks. *J. Am. Chem. Soc.* **133**, 12926–12929 (2011).
24. W.-J. Li, M. Tu, R. Cao, R. A. Fischer, Metal–organic framework thin films: Electrochemical fabrication techniques and corresponding applications & perspectives. *J. Mater. Chem. A* **4**, 12356–12369 (2016).
25. F. SciFinder, Calculated using Advanced Chemistry Development (ACD/Labs) Software V11. 02 (© 1994–2012 ACD/Labs).
26. D. A. Newsome, D. S. Sholl, Molecular dynamics simulations of mass transfer resistance in grain boundaries of twinned zeolite membranes. *J. Phys. Chem. B* **110**, 22681–22689 (2006).
27. Y. Liu, Y. Peng, N. Wang, Y. Li, J. H. Pan, W. Yang, J. Caro, Significantly enhanced separation using ZIF-8 membranes by partial conversion of calcined layered double hydroxide precursors. *ChemSusChem* **8**, 3582–3586 (2015).
28. O. Shekhah, R. Swaidan, Y. Belmabkhout, M. du Plessis, T. Jacobs, L. J. Barbour, I. Pinnau, M. Eddaoudi, The liquid phase epitaxy approach for the successful construction of ultra-thin and defect-free ZIF-8 membranes: Pure and mixed gas transport study. *Chem. Commun.* **50**, 2089–2092 (2014).
29. W. J. W. Bakker, L. J. P. Van Den Broeke, F. Kapteijn, J. A. Moulijn, Temperature dependence of one-component permeation through a silicalite-1 membrane. *AIChE J.* **43**, 2203–2214 (1997).

30. T. C. T. Pham, T. H. Nguyen, K. B. Yoon, Gel-free secondary growth of uniformly oriented silica MFI zeolite films and application for xylene separation. *Angew. Chem. Int. Ed.* **52**, 8693–8698 (2013).
31. P. Krokidas, M. Castier, I. G. Economou, Computational study of ZIF-8 and ZIF-67 performance for separation of gas mixtures. *J. Phys. Chem. C* **121**, 17999–18011 (2017).
32. M. G. Martin, J. I. Siepmann, Transferable potentials for phase equilibria. 1. United-atom description of n-alkanes. *J. Phys. Chem. B* **102**, 2569–2577 (1998).
33. C. D. Wick, M. G. Martin, J. I. Siepmann, Transferable potentials for phase equilibria. 4. United-atom description of linear and branched alkenes and alkylbenzenes. *J. Phys. Chem. B* **104**, 8008–8016 (2000).
34. S. E. Feller, Y. Zhang, R. W. Pastor, B. R. Brooks, Constant pressure molecular dynamics simulation: The Langevin piston method. *J. Chem. Phys.* **103**, 4613–4621 (1995).
35. L. Ding, Y. Wei, L. Li, T. Zhang, H. Wang, J. Xue, L.-X. Ding, S. Wang, J. Caro, Y. Gogotsi, MXene molecular sieving membranes for highly efficient gas separation. *Nat. Commun.* **9**, 155 (2018).
36. I. G. Tironi, R. Sperb, P. E. Smith, W. F. van Gunsteren, A generalized reaction field method for molecular dynamics simulations. *J. Chem. Phys.* **102**, 5451–5459 (1995).
37. N. Hara, M. Yoshimune, H. Negishi, K. Haraya, S. Hara, T. Yamaguchi, Diffusive separation of propylene/propane with ZIF-8 membranes. *J. Membr. Sci.* **450**, 215–223 (2014).
38. Q. Liu, N. Wang, J. Caro, A. Huang, Bio-inspired polydopamine: A versatile and powerful platform for covalent synthesis of molecular sieve membranes. *J. Am. Chem. Soc.* **135**, 17679–17682 (2013).
39. F. Hillman, J. M. Zimmerman, S.-M. Paek, M. R. A. Hamid, W. T. Lim, H.-K. Jeong, Rapid microwave-assisted synthesis of hybrid zeolitic–imidazolate frameworks with mixed metals and mixed linkers. *J. Mater. Chem. A* **5**, 6090–6099 (2017).
40. D. Liu, X. Ma, H. Xi, Y. S. Lin, Gas transport properties and propylene/propane separation characteristics of ZIF-8 membranes. *J. Membr. Sci.* **451**, 85–93 (2014).
41. Y. Pan, T. Li, G. Lestari, Z. Lai, Effective separation of propylene/propane binary mixtures by ZIF-8 membranes. *J. Membr. Sci.* **390–391**, 93–98 (2012).
42. J. Yu, Y. Pan, C. Wang, Z. Lai, ZIF-8 membranes with improved reproducibility fabricated from sputter-coated ZnO/alumina supports. *Chem. Eng. Sci.* **141**, 119–124 (2016).
43. A. J. Brown, N. A. Brunelli, K. Eum, F. Rashidi, J. R. Johnson, W. J. Koros, C. W. Jones, S. Nair, Interfacial microfluidic processing of metal-organic framework hollow fiber membranes. *Science* **345**, 72–75 (2014).
44. Y. Hu, J. Wei, Y. Liang, H. Zhang, X. Zhang, W. Shen, H. Wang, Zeolitic imidazolate framework/graphene oxide hybrid nanosheets as seeds for the growth of ultrathin molecular sieving membranes. *Angew. Chem. Int. Ed.* **55**, 2048–2052 (2016).
45. H. T. Kwon, H.-K. Jeong, In situ synthesis of thin zeolitic–imidazolate framework ZIF-8 membranes exhibiting exceptionally high propylene/propane separation. *J. Am. Chem. Soc.* **135**, 10763–10768 (2013).
46. H. T. Kwon, H.-K. Jeong, Improving propylene/propane separation performance of Zeolitic-Imidazolate framework ZIF-8 Membranes. *Chem. Eng. Sci.* **124**, 20–26 (2015).
47. E. Shamsaei, X. Lin, L. Wan, Y. Tong, H. Wang, A one-dimensional material as a nano-scaffold and a pseudo-seed for facilitated growth of ultrathin, mechanically reinforced molecular sieving membranes. *Chem. Commun.* **52**, 13764–13767 (2016).
48. E. Shamsaei, X. Lin, Z.-X. Low, Z. Abbasi, Y. Hu, J. Z. Liu, H. Wang, Aqueous phase synthesis of ZIF-8 membrane with controllable location on an asymmetrically porous polymer substrate. *ACS Appl. Mater. Interfaces* **8**, 6236–6244 (2016).
49. J. J. Krol, M. Boerrigter, G. H. Koops, Polyimide hollow fiber gas separation membranes: Preparation and the suppression of plasticization in propane/propylene environments. *J. Membr. Sci.* **184**, 275–286 (2001).
50. S. Bai, S. Sridhar, A. A. Khan, Metal-ion mediated separation of propylene from propane using PPO membranes. *J. Membr. Sci.* **147**, 131–139 (1998).
51. S. Sridhar, A. Khan, Simulation studies for the separation of propylene and propane by ethylcellulose membrane1. *J. Membr. Sci.* **159**, 209–219 (1999).
52. C. Staudt-Bickel, W. J. Koros, Olefin/paraffin gas separations with 6FDA-based polyimide membranes. *J. Membr. Sci.* **170**, 205–214 (2000).
53. K. Tanaka, A. Taguchi, J. Hao, H. Kita, K. Okamoto, Permeation and separation properties of polyimide membranes to olefins and paraffins. *J. Membr. Sci.* **121**, 197–207 (1996).
54. M. L. Chng, Y. Xiao, T.-S. Chung, M. Toriida, S. Tamai, Enhanced propylene/propane separation by carbonaceous membrane derived from poly (aryl ether ketone)/2, 6-bis (4-azidobenzylidene)-4-methyl-cyclohexanone interpenetrating network. *Carbon* **47**, 1857–1866 (2009).
55. X. Ma, B. K. Lin, X. Wei, J. Kniep, Y. S. Lin, Gamma-alumina supported carbon molecular sieve membrane for propylene/propane separation. *Ind. Eng. Chem. Res.* **52**, 4297–4305 (2013).
56. K.-i. Okamoto, S. Kawamura, M. Yoshino, H. Kita, Y. Hirayama, N. Tanihara, Y. Kusuki, Olefin/paraffin separation through carbonized membranes derived from an asymmetric polyimide hollow fiber membrane. *Ind. Eng. Chem. Res.* **38**, 4424–4432 (1999).
57. I. G. Giannakopoulos, V. Nikolakis, Separation of propylene/propane mixtures using faujasite-type zeolite membranes. *Ind. Eng. Chem. Res.* **44**, 226–230 (2005).
58. M. Kanezashi, W. N. Shazwani, T. Yoshioka, T. Tsuru, Separation of propylene/propane binary mixtures by bis (triethoxysilyl) methane (BTESM)-derived silica membranes fabricated at different calcination temperatures. *J. Membr. Sci.* **415–416**, 478–485 (2012).
59. H. T. Kwon, H.-K. Jeong, A. S. Lee, H. S. An, J. S. Lee, Heteroepitaxially grown zeolitic imidazolate framework membranes with unprecedented propylene/propane separation performances. *J. Am. Chem. Soc.* **137**, 12304–12311 (2015).

Acknowledgments: We thank A. Feldhoff for helpful suggestions on the experiments. **Funding:** We gratefully acknowledge the funding from the Natural Science Foundation of China (21536005, 51621001, 21506066, and 21606086), NSFC-DFG (GZ-678), the Natural Science Foundation of the Guangdong Province (2014A030312007), and Guangdong Natural Science Funds for Distinguished Young Scholar (2017A030306002). J.C. thanks the 1000 Talents Program of the Chinese government. **Author contributions:** S.Z., Y.W., H.W., and J.C. conceived the idea and designed the experiments. S.Z. synthesized the materials and carried out most of the characterization. S.Z. and Q.H. performed the gas separation experiments. S.Z. and Y.W. analyzed the results. L.L. and Y.D. contributed to the MD simulations. L.-X.D. and L.Z. guided the electrochemical characterization. J.X. guided the refinement of the XRD results. S.Z., Y.W., H.W., and J.C. wrote the manuscript. **Competing interests:** The authors declare that they have no competing interests. **Data and materials availability:** All data needed to evaluate the conclusions in the paper are present in the paper and/or the Supplementary Materials. Additional data related to this paper may be requested from the authors.

Submitted 10 May 2018
Accepted 17 September 2018
Published 26 October 2018
10.1126/sciadv.aau1393

Citation: S. Zhou, Y. Wei, L. Li, Y. Duan, Q. Hou, L. Zhang, L.-X. Ding, J. Xue, H. Wang, J. Caro, Paralyzed membrane: Current-driven synthesis of a metal-organic framework with sharpened propene/propane separation. *Sci. Adv.* **4**, eaau1393 (2018).

Paralyzed membrane: Current-driven synthesis of a metal-organic framework with sharpened propene/propane separation

Sheng Zhou, Yanying Wei, Libo Li, Yifan Duan, Qianqian Hou, Lili Zhang, Liang-Xin Ding, Jian Xue, Haihui Wang and Jürgen Caro

Sci Adv **4** (10), eaau1393.
DOI: 10.1126/sciadv.aau1393